Frangible Roof Joint Behavior of Cylindrical Oil Storage Tanks Designed to API 650 Rules

Z. Lu

D. V. Swenson

D. L. Fenton

Mechanical Engineering Department,
Durland Hall,
Kansas State University,
Manhattan, KS 66506

This paper presents the results of an investigation into the frangible joint behavior of tanks designed to API 650 rules. In such tanks, the roof-to-shell joint is intended to fail in the event of overpressurization, venting the tank and containing any remaining fluid. The reasoning behind present API design formulas is reviewed. Combustion analyses, structural analyses, and the results of testing are presented. Results show that higher pressures are reached before frangible joint failure than predicted by the present API 650 calculation. One consequence is that (for empty tanks) uplift of the bottom can be expected to occur more frequently than predicted using API 650. However, uplift does not necessarily mean bottom failure. Instead, the relative strength of the shell-to-bottom and roof-to-shell joints will determine failure. This ratio is larger for larger tanks. Recommendations are made as to possible changes in the design approach of API 650.

Introduction

Vertical, cylindrical, above-ground, fixed roof storage tanks are widely used in the petroleum and chemical industries. Due to filling and emptying of the tanks, the vapor above the liquid surface inside the tank may be within its flammability limits. Ignition of this vapor can cause sudden overpressurization and can lead to the catastrophic loss of tank integrity.

API 650 (American Petroleum Institute, 1993) provides design criteria for fluid storage tanks used to store flammable liquids. To prevent shell or bottom failure, the rules in API 650 are intended to ensure that the frangible roof-to-shell joint fails before failure occurs in the tank shell or the shell-to-bottom joint. Failure of the frangible roof-to-shell joint provides a large venting area and reduces the pressure in the tank. An excellent description of tank failures and application of the design rules is given by Morgenegg (1978). Experience has shown that a roof-to-shell joint so designed may not perform as intended, especially for smaller tanks (Prager, 1991).

This paper is a description of an evaluation of the present design criteria. The project included calculations of predicted pressure loads due to deflagration, structural analyses of storage tanks, static testing of joints and scale models, and dynamic tests of scale models. Finally, the knowledge gained was integrated into a computer program to design and analyze tanks. Based on these evaluations, recommendations are made as to possible changes in the approach used in API 650.

API 650 Design Rules for Frangible Roof Joints

The storage tanks addressed in this research include the typical tanks seen in oil refineries and chemical plants (Fig. 1). The tanks are cylindrical with conical roofs. The roof slope is limited by API 650 to a rise not greater than 2 in. in 12 in. The tanks typically have a flat floor that rests on a sand foundation, with a hard concrete ringwall at the periphery of the bottom. The tanks are manufactured in the field using fillet or butt-welded plates. Overlapping joints (with fillet welds) are typical on the roof and floor. Butt welds are used for the shell. Diameters of the tanks of interest range from 10 to over 200 ft (3 to 60 m), with heights of 10 to 60 ft (3 to 18 m). The material used in construction is steel, with yield strengths ranging from 30,000 to 60,000 psi (200 to 400 MPa).

Several sections of the API 650 code address the design of a frangible roof joint for supported cone roofs. The most important rule is the area inequality rule, which states that frangible roof joint behavior will be expected if the cross-sectional area at the roof-to-shell junction does not exceed

$$A = \frac{0.153W}{30{,}800 \tan \theta} \tag{1}$$

All other design rules support or follow from this requirement. The area inequality rule is derived using static equilibrium and the undeformed geometry of the tank. The derivation assumes the upward pressure on the roof is equal to the weight of the tank (incipient uplift). The associated inward radial load component is set equal to the load necessary to cause yielding of the compression ring. This rule is intended to ensure that yielding of the compression ring will occur before uplift of the tank. Yielding and subsequent loss of stiffness are expected to cause buckling of the compression ring, followed by gross deformation of the roof and shell, and associated failure of the roof-to-shell weld. As discussed later, our testing confirms that this is the mode in which failure occurs.

The cross section area of the compression ring at the roof-to-shell joint is defined by parameters W_c and W_h, as shown in Fig. 2. Because of the methods used to calculate W_c and W_h and the simplified analysis of the joint, failure is predicted by API 650 at lower pressures than predicted by closed-form analysis, finite element calculations, and as observed in experiment. The implications are discussed later.

Combustion Analysis

To evaluate the structural response of the tank to combustion, a numerical model was developed to predict the pressure rise inside the tank. Experimental evidence (Barnett and Hibbard, 1957) and the present testing support the assumption that combustion will be by deflagration rather than a detonation. A deflagration is characterized by a relatively low burning velocity (open air flame front velocity on the order of 30 ft/s (9 m/s)) and small pressure rise across the combustion wave. The analysis assumes that the combustion wave will burn as a radial

Contributed by the Pressure Vessels and Piping Division for publication in the JOURNAL OF PRESSURE VESSEL TECHNOLOGY. Manuscript received by the PVP Division, December 19, 1994; revised manuscript received October 13, 1995. Associate Technical Editor: M. Prager.

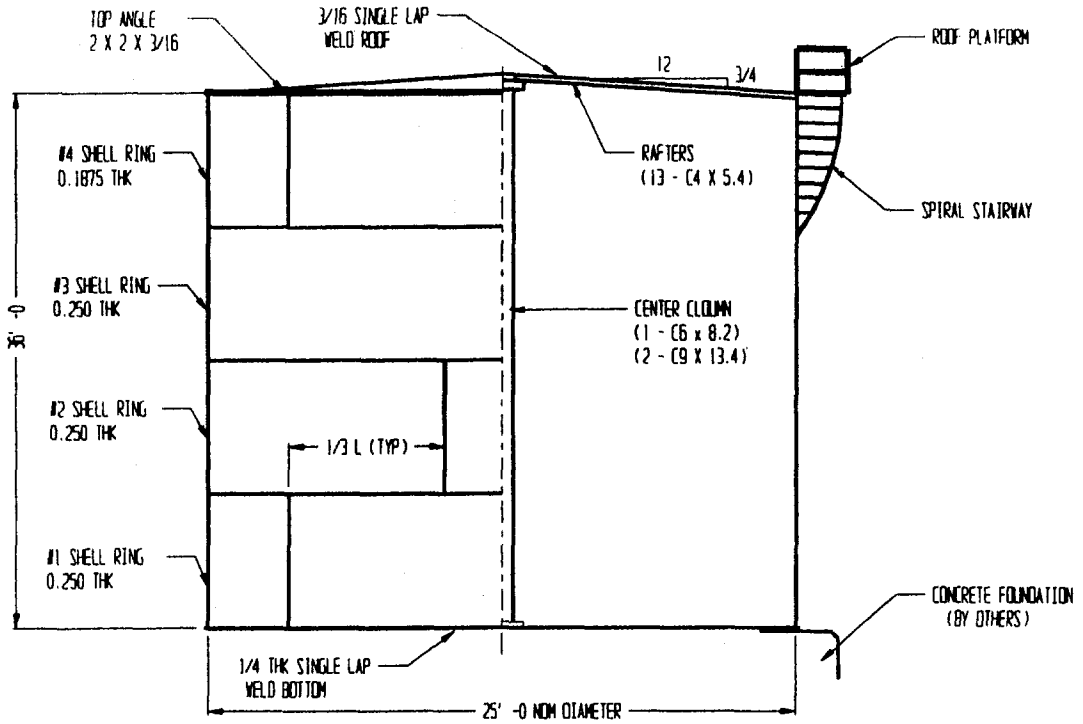

Fig. 1 Schematic of typical tank

deflagration, having a smooth spherical-shaped flame front from a point source ignition.

To simplify the numerical model, the calculation of the adiabatic constant volume flame temperature uses chemical equilibrium (Ferguson, 1986) instead of chemical kinetics. The tank is assumed to be adiabatic and the structure of the tank rigid. The analysis also assumes no net effect due to radiation heat transfer between the flame front and wall of the tank.

To calculate a pressure rise during a time increment, the volume swept out by the flame front is the outer shell of a sphere or partial sphere. The thickness of the shell equals the burning velocity multiplied by a time increment. The volume swept by the flame front is then allowed to expand, causing the reactants and products to compress until the pressure inside the tank is uniform. After the pressure inside the tank is balanced, time is incremented and the process repeated until all the reactants are burned.

Structural Analyses

A range of analyses were performed to help understand tank behavior and to predict test results. The axisymmetric and 3-D analyses discussed in this section were made using the ANSYS (Swanson Analysis Inc., 1994) finite element code. In the following discussion, only summaries of the analyses will be given.

Scoping Analyses of Full-Scale Tanks. Before testing, scoping analyses of full-scale tanks were performed to understand tank behavior. Two generic tanks were chosen for the initial full-scale scoping analyses: a "small" tank with a diameter of 25 ft (7.6 m) and height of 36 ft (11.0 m) and a "large" tank with a diameter of 140 ft (42.7 m) and height of 40 ft (12.2 m).

A fundamental calculation is a static linear elastic analysis of the tanks under internal pressure. Figure 3 shows the calculated circumferential stresses near the roof joint in a 25-ft- (7.6-m-) dia tank for a range of roof slopes. For comparison, a closed-form solution is also plotted. The combination of roof lifting and constraint at the top angle results in compressive stresses in the roof-to-shell joint. An important feature is that, as the roof slope increases, the peak compressive stress becomes smaller and more local to the joint. As a consequence, a roof with a larger slope will be stronger than a flatter roof. It should be noted that elastic large displacement and small displacement analyses gave essentially the same results in the region of the compression ring.

For comparison with the compressive area calculation in API 650, Fig. 3 includes the calculations of W_h and W_c as specified in API 650 Appendix F. As can be seen, selecting the appropriate area is not obvious. Selecting too small values for W_h and W_c gives too small an area for the compression ring. This leads to a prediction of frangible joint failure when it would not actually occur. As a result, pressures in the tank may rise above those predicted using API 650 calculations.

Axisymmetric modal analyses were performed to determine the natural frequencies of the tanks and to evaluate whether dynamic calculations were required to capture the tank response to combustion. The lowest mode is associated with lifting of the roof, with the lowest calculated frequencies for the small and large tanks 7.7 and 0.95 Hz, respectively. A fast Fourier transform (FFT) of the pressure loading gave the dominant loading frequencies as 1.0 Hz for the small tank and 0.5 Hz for

Nomenclature

A = area resisting compressive force, in^2 (API 650)
θ = angle of roof with horizontal, deg (API 650)
W = total weight of shell and any framing (but not roof plates) supported by shell and roof (API 650)
W_c = maximum width of participating shell, in. (API 650)
W_h = maximum width of participating roof, in. (API 650)

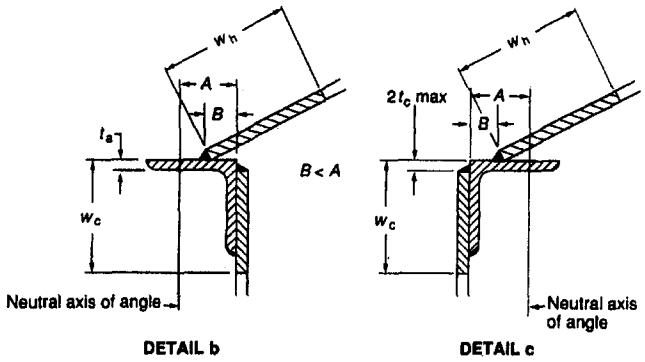

Fig. 2 Permissible details of some compression rings (from API 650)

the large tank. Because the frequencies of pressure rise in the tanks are significantly lower than the natural frequency of the tanks (especially for the small tank), dynamic effects are not significant before failure initiation and static analyses were judged to be appropriate.

A three-dimensional model of the joint was used to determine the elastic buckling mode and the critical load. Elastic buckling can occur predominantly in the roof where the circumferential stresses are compressive. As the roof slope increases, both the critical load and the mode increase significantly. However, elastic buckling does not imply failure. Instead, the post-buckling structure remains stable, as confirmed by our experiments. Elastic buckling of roof plates just means that the compressive circumferential stress in the roof is reduced; thus, the calculation of elastic buckling loads (Yoshida and Myoshi, 1992) is not sufficient to evaluate joint failure. The radial tensile stress is still applied to the compression ring, and, if increased, will eventually cause yielding of the compression ring.

Analyses of Model Tanks Tested Dynamically. Axisymmetric large displacement analyses were performed of the model tanks that were dynamically tested (see Testing section for tank details). The model used a bilinear material, with Young's modulus of 30×10^6 psi (207 GPa), Poisson's ratio of 0.3, a yield stress of 36,000 psi (248 MPa), and a plastic modulus of 600,000 psi (4.1 GPa). Results were scaled to the later measured yield stress of 49,000 psi (340 MPa). By resting the bottom on compression-only elements, the support of the tank was modeled as an elastic foundation.

For the model tank, through-thickness yielding of the compression joint occurred at about 6.1 psi (31 kPa). Also, the mid-plane equivalent stress at the bottom shell was of the same order as that of the top shell. As a result of this analysis, the

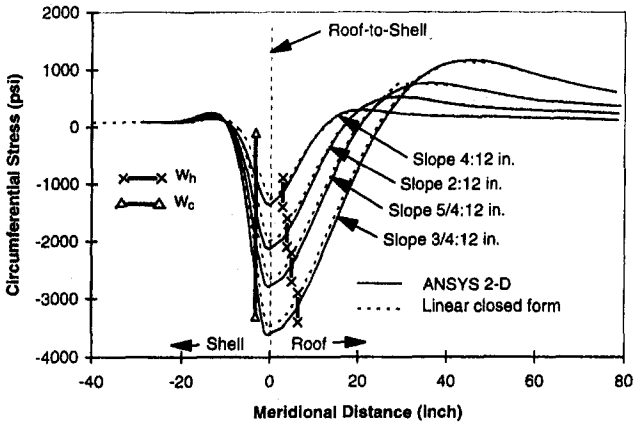

Fig. 3 Circumferential stress in 25-ft-dia tank due to 0.1-psi pressure

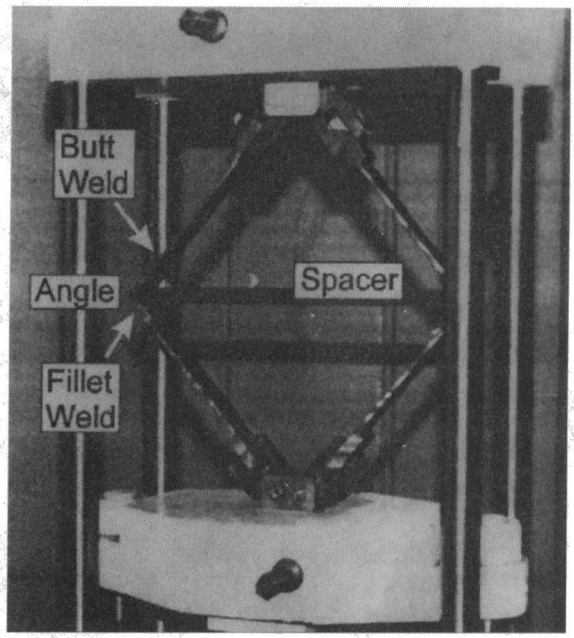

Fig. 4 Joint specimen testing

bottom joint was reinforced to ensure failure of the top joint during the test.

One of the dynamically tested models had a stitch weld instead of a continuous weld. Each stitch was 2 in. (5.1 cm) long with 18 welds around the circumference, for a spacing of about 16 in. (40.6 cm). The 3-D finite element model showed an equivalent stress equal to the yield stress in the top angle near the stitch weld when the internal pressure was 1.6 psi (11 kPa). An alternate upper-bound failure prediction was made by assuming that the circumferential stress near the joint of the stitch-welded tank was equal to that of a continuously welded tank at the same pressure, but the radial force on the shell was carried only by the portion of welded joint. This prediction indicated failure at about 4 psi (27 kPa).

Testing

Joint Details. Testing of joint details was used to evaluate sensitivity of the failure to weld dimensions. Welded joint specimens were tested in pairs, with and without a spacer that prevented rotation at the weld (Fig. 4). When rotation was constrained, the $\frac{3}{16}$-in. (4.7-mm) welds sustained loads of 4000 lb/in. (0.7 MN/m), but when rotation was allowed, the failure load dropped to 65 lb/in. (11 kN/m). This testing showed the joint may be stronger than the plate unless rotation at the weld occurs.

Static Test of Small-Scale Model Tanks. Two small-scale models were constructed of 20-gage sheet (0.036 in. (0.91 mm)) with a measured yield stress of 38,000 psi (260 MPa). The tanks had a diameter of 4 ft (1.2 m), with shells 2 ft (0.61 m) tall. One tank was constructed with a flat roof and the other with a roof that had a slope of 4 in. in 12 in. These dimensions were chosen so as to give extremes of elastic buckling behavior. Finite element analysis predicted that elastic buckling should occur at 0.85 psi (6 kPa) for the flat roof model and yielding of the compression ring was predicted at 1.5 psi (10 kPa). For the model with a large roof slope, elastic buckling was predicted at 7 psi (48 kPa) and yielding at 4 psi (27 kPa).

For the tank with the flat roof, elastic buckling occurred in the tank roof below 1 psi (7 kPa) (the exact pressure is not known due to initial difficulties in running the test). This elastic buckling was very pronounced. About 16 waves formed around

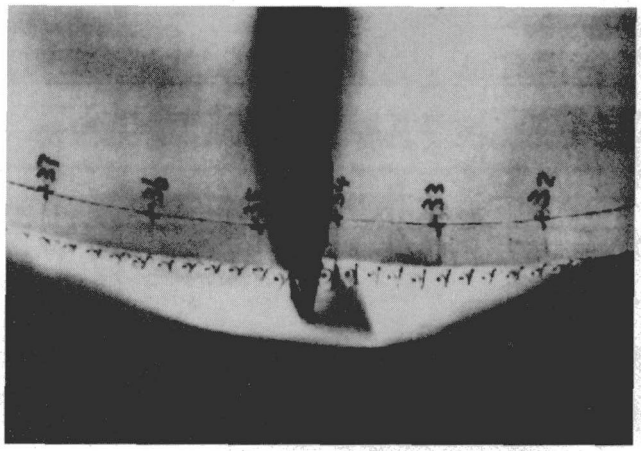

Fig. 5 First large inelastic buckle on flat roof tank at 1.2 psi

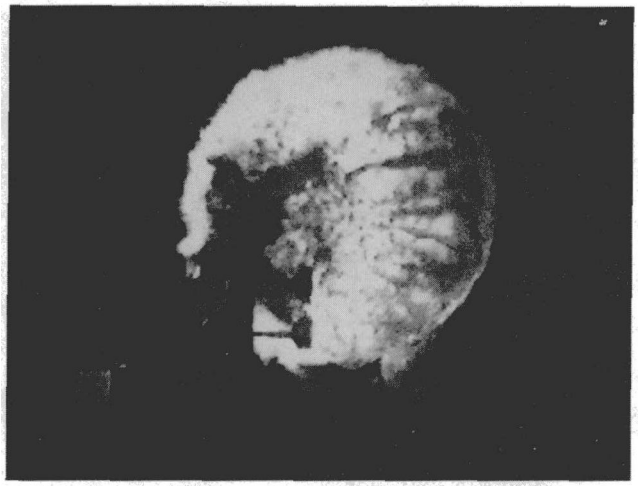

Fig. 6 Open air deflagration test at night

the entire circumference with an amplitude of about 0.1 in. (2.5 mm). An important point is that this elastic buckling did not result in significant deformation of the roof-to-shell joint. In fact, the buckling was stable and we were able to continue to load the tank. At a pressure of about 1.2 psi (8 kPa), a large inelastic buckle formed at the joint (Fig. 5). This is approximately the pressure at which yielding of the ring was expected. An increase in pressure to 1.5 psi (10 kPa) resulted in the formation of four buckles spaced about 90 deg apart. The large rotation caused by these buckles would most likely have failed a welded joint. The sequence of elastic buckling followed by yielding of the compression ring matches the analytical prediction.

The test with the sloped roof was performed in a similar manner. However, as predicted, no elastic buckling was observed. The roof was smooth and without buckles until 4.0 psi (27 kPa), at which pressure about 30 sharp ridges formed close to the roof joint. At a pressure of about 5.5 psi (38 kPa), large inelastic buckles formed at the roof-to-shell joint.

Dynamic Test of Model Tanks. Two model tanks with different roof joints were tested dynamically. The internal burning was simulated by ignition of an air-methane gas mixture. One of the two tanks represented a standard design, while the second one had a stitch-welded joint between the top angle and roof.

The design of the scale model tanks was based on existing oil storage tanks, but with reduced scale geometry. The tanks were 7.5 ft (2.3 m) in diameter and 8 ft (2.4 m) high, with a thickness of $\frac{1}{8}$ in. (3.2 mm) for the shell and roof. The tanks were made of ASTM A36, with a measured yield stress of 49,000 psi (340 MPa), ultimate stress of 57,000 psi (390 MPa), and Young's modulus of 28×10^6 psi (190 GPa). Rafters were included in the tanks, both to be representative of a typical tank and to prevent distortion of the roof during transportation.

The combustible vapor was contained in a weather balloon inside the tank. This balloon was filled with 90 cu ft (2.5 m^3) of methane and air mixture at stoichiometric conditions. A point ignition source located at the center of the balloon was used to ignite the methane.

To verify that combustion was by deflagration, four open-air tests of balloons were performed. In all cases, the combustion occurred by deflagration. About $\frac{1}{3}$ s was required from ignition of the air-methane mixture until the balloon burst, revealing a spherical combustion front, as shown in Fig. 6.

The continuously welded tank was tested first. As can be seen in the videos and high-speed films, failure was initiated by one local buckle at the top joint. The buckling bent the roof plate sharply, followed by local failure of the weld. Failure then proceeded from the initiation location in both directions around the tank. The failure continued until only 4 ft (1.2 m) of weld remained intact. The pressure on the opened roof pushed the tank to one side, broke the anchors, and nearly tipped the tank over. In this test all four of the rafters in compression were buckled and one of them detached from the shell. The two rafters in tension were both detached from the rafter gussets. Figure 7 shows the tank after test.

The failure of the joint of the continuously welded tank was mainly in the base material of the roof plate adjacent to the weld, with portions of the top angle broken. This confirms the tendency of welders to make the weld stronger than needed or of possible reduction of strength in the heat-affected zone.

In the test of the stitch-welded tank, the roof completely separated from the tank due to failure of the stitch welds. A single stitch failed first, followed by the adjacent welds. The roof was "blown off" the tank and distortion of the shell of the stitch-welded tank was much less than that of the continuously welded tank. All rafters remained intact, without any buckling.

During the test of the continuously welded tank, the pressure transducer failed, so no direct pressure readings are available. The peak pressure can be estimated using Fig. 8, which shows a measured strain near the joint, the predicted pressure, and the corresponding predicted strains from finite element analysis (dots at pressures for which the strains were calculated). The strain readings are initially proportional to the pressure rise, with the severe deformation occurring at about 6 to 8 psi (40 to 55 kPa). Considering that venting is not instantaneous following the initial failure of the joint, we believe the peak pressure was between 8 and 10 psi (55 and 69 kPa). This is rein-

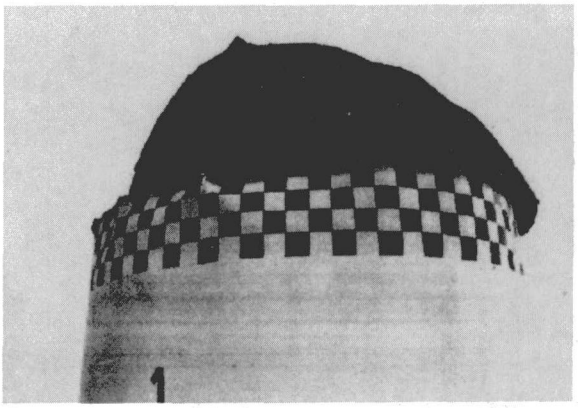

Fig. 7 Continuously welded tank after test

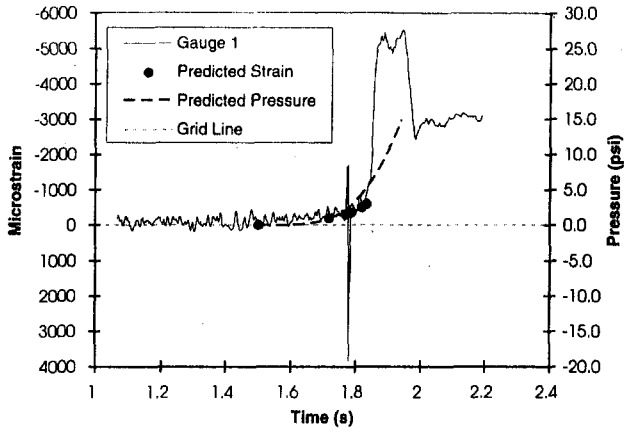

Fig. 8 Strain and pressure readings of continuously welded tank

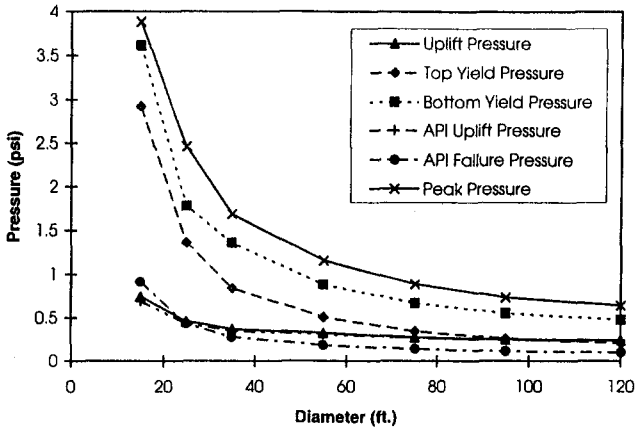

Fig. 10 Critical pressures for 45-ft high empty tanks

forced by the comparison between the predicted strains at 5.5 psi (38 kPa) and the measured strains.

Results for the stitch-welded tank are given in Fig. 9, with the measured pressure curve superimposed. It can be seen that for this gage, the deformation of the shell was in proportion to the pressure until about 5 psi (34 kPa). Beyond that point, the failure of the stitch weld and the stress redistribution of the shell caused uneven deformation.

These dynamic tests provided evidence that failure of the top joint is by inelastic buckling following yielding of the compression ring. Also, because venting does not occur instantaneously following failure, the peak pressure may be larger than the pressure at failure initiation.

Integration of Analyses and Experiments

Using the information learned in analysis and testing, a computer program, API-Tank, was written and used to predict the pressures of the different tank failure modes for a range of tank heights and diameters. The critical pressures include bottom uplift, top yield (compression ring yield), bottom yield (bottom shell yield), the peak value during a combustion/failure calculation, and the API predictions for uplift and failure. The development of API-Tank is described in Lu and Swenson (1994). Results are shown for 45-ft (13.7-m) high empty tanks in Fig. 10 and for full tanks in Fig. 11.

The results show that for empty tanks, the uplift pressure predicted by API 650 and the finite element calculation are essentially identical. In most cases, some uplift is expected before failure initiation at the roof-to-shell joint.

The failure (yielding) pressures of the roof-to-shell joint predicted using API-Tank are significantly higher than those obtained using the API 650. That is, API 650 predicts top joint failure at pressures that do not cause yielding in the finite element analysis. The API-Tank calculations are supported by analytic solutions and ANSYS results. Since the roof-to-shell joint failure is an expected design condition to relieve pressure in the tank, a prediction of failure below pressures at which it will actually occur is not desirable and the API 650 calculation is not conservative in that respect. However, this does not imply that tanks designed to API 650 rules will fail at the bottom joint first. Instead, it is necessary to examine the relative strengths of the joints.

In all cases examined, the pressure to cause yielding of the shell-to-bottom joint was larger than that to cause yielding at the roof-to-shell joint. However, the margin between the two pressures is a function of tank dimension. For instance, for a 45-ft (13.7-m) high, 15-ft- (4.6-m-) dia empty tank, the bottom yield pressure is 3.6 psi (25 kPa) and the top yield pressure is 2.9 psi (20 kPa), giving a design factor of 1.2. However, for a 45-ft (13.7-m) high, 95-ft- (30-m-) dia empty tank, the bottom yield pressure is 0.55 psi (3.8 kPa) and the top yield pressure is 0.26 psi (1.8 kPa), for a design factor of 2.12. Tanks filled with fluid require larger pressures before uplift and require larger pressures before yielding at the shell-to-bottom joint; therefore, they have a larger design factor.

The peak pressure calculation has the most uncertainty of the pressures shown on the figures. Many assumptions were made in calculating the venting area and process during failure. However, if the frangible joint yield and bottom joint yield occur at approximately the same pressure, it is reasonable to expect a

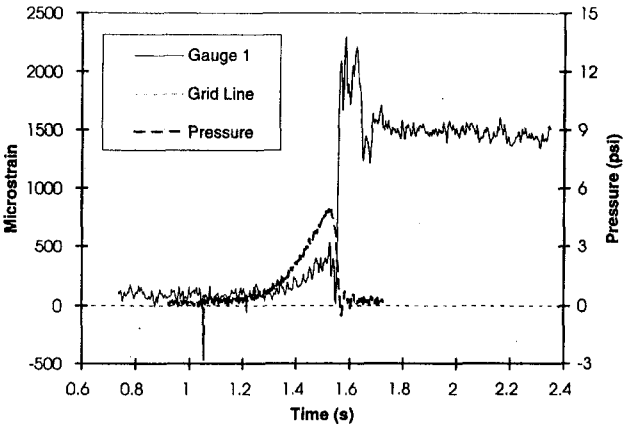

Fig. 9 Strain and pressure reading of stitch welded tank

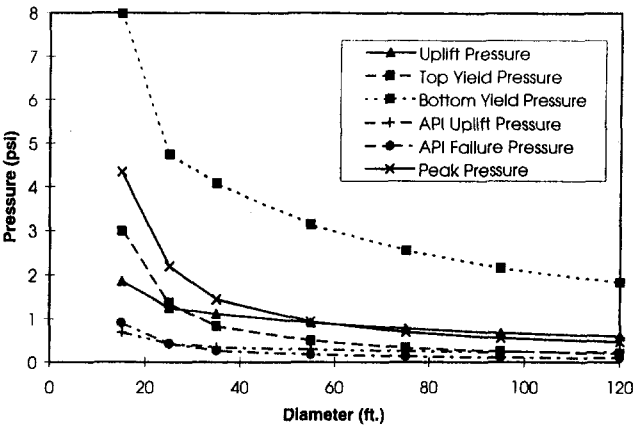

Fig. 11 Critical pressures for 45-ft high full tanks

peak pressure that will exceed the frangible joint failure initiation pressure and increases the potential for failure of the bottom joint. If there is a significant margin between the two failure pressures, sufficient venting should occur to prevent failure of the bottom joint.

The results confirm the field observations that frangible joints perform well for large tanks, but may not always fail as desired for smaller tanks. The design margin between bottom yield pressure and top yield pressure is much larger for large tanks. The results also are consistent with the observation of uplift before top joint failure as reported by Morgenegg (1978).

Conclusions

With respect to derivation and applicability of the API 650 design rules:

1 API 650 design equations for frangible roof joints are derived based on compressive yielding of the roof-to-shell joint and simple equilibrium analysis.

2 The failure pressure calculated using API 650 rules is significantly lower than that predicted using finite element analysis or observed in testing.

3 The uplift pressure calculated using API 650 rules is very close to that calculated with finite element analysis.

With respect to the combustion analysis:

1 The assumption that combustion of the mixture occurs by deflagration was supported by test data.

2 The combustion process is relatively slow, taking at least several tenths of a second to reach pressures that can fail a typical tank. As a result, the tanks are expected to respond statically to the deflagration loading.

With respect to testing:

1 The fillet weld on the roof-to-shell joint tends to be as strong as the plates. Tearing failure was observed both in the weld and in the angle and roof during testing.

2 Elastic buckling of the roof does not cause failure, but leads to a new stable configuration. Loading can then continue until yielding of the ring occurs.

3 Failure of the continuously welded tank occurred as expected, initiated by a local inelastic buckle, followed by general failure of the weld.

4 The rafters had no apparent effect on failure pressure or location for either tank.

5 Failure of the stitch welded tank occurred at a lower pressure than for the continuously welded tank. The roof completely detached, with much less distortion of the upper shell.

With respect to the analysis of failure modes:

1 Empty tanks with diameters less than 100 ft (30 m) may uplift before yielding at the top joint (frangible roof-to-shell failure). However, uplift at the bottom does not necessarily constitute failure of the bottom joint.

2 The relative strength of the roof-to-shell joint and shell-to-bottom joint is a strong function of the liquid level when the overpressurization occurs. The weight of the liquid holds the bottom from being uplifted and reduces the stress at the shell-to-bottom joint.

3 In all calculations, the frangible joint failure pressure was smaller than the bottom yield pressure, but the design margin (ratio of bottom yield pressure to top joint failure pressure) is larger for large-diameter empty tanks.

Recommendations

1 The equations used in API 650 to predict yielding at the compression ring should be improved. One approach would be to use the linear elastic analytic solution for a cylinder/cone to calculate the stresses in the joint. Such equations could be easily calculated using a spreadsheet.

2 Uplift is probably too restrictive a criterion for design and should be replaced by an alternate criterion.

3 Perhaps as an alternate to an uplift criterion, the relative strengths of the bottom and frangible joints could be used in the margin evaluation. For example, the criterion could state that the bottom yield pressure must be twice as large as the top yield pressure (frangible joint failure). This would ensure that the frangible joint would fail first, while still allowing some uplift to occur.

4 The foregoing approach could be expanded to include other possible failure modes, such as fracture due to manufacturing defects. The criterion could compare the failure pressure due to possible defects with the frangible joint failure pressure and require, for instance, that the defect failure pressure be twice that of the frangible joint failure pressure.

5 Consideration needs to be given to the liquid level at which the design margin evaluation is done. An empty tank has a lower bottom joint failure pressure and a smaller bottom to frangible joint strength design margin, but the consequence of a bottom failure is minor. In contrast, a full tank has a higher bottom failure pressure and higher design margin, but worse consequences if failure occurs.

Acknowledgments

This work was supported by the Pressure Vessel Research Council (Committee on Dynamic Analysis and Testing, and Shells and Ligaments Committee) and the American Petroleum Institute. We thank Jerry Bitner, Greg Hollinger, Martin Prager, Guido Karcher, Richard Basile, and J. C. Thompson for useful discussions. We especially appreciate the support of Texaco, El Dorado Plant, and Ace Construction in construction of the tanks. Mark Devries, undergraduate honors student, and Asif Ghori, graduate student, helped in the testing of the tanks. The Agriculture Department at Kansas State provided the test site. The Kinesiology Departments at Kansas State and the University of Kansas provided the high-speed camera equipment and technical support.

References

American Petroleum Institute, 1993, "API Standard 650: Welded Steel Tanks for Oil Storage," 9th Edition, Washington, DC.

Barnett, H. C., and R. R. Hibbard, 1957, "Basic Considerations in the Combustion of Hydrocarbon Fuels With Air," Rept. 1300, Propulsion Chemistry Division, Lewis Flight Propulsion Lab., NASA, Cleveland, OH.

Ferguson, C. R., 1986, *Internal Combustion Engines,* John Wiley and Sons, New York, NY.

Lu, Zhi, and Swenson, Daniel, 1994, "User's Manual for API-Tank: A Program for the Analysis of Storage Tanks with Frangible Roof Joints," Manual Release 1.0, Mechanical Engineering Dept., Kansas State University, Manhattan, KS.

Morgenegg, E. E., 1978, "Frangible Roof Tanks," *Proceedings, American Petroleum Institute,* Refin. Dep., Midyear Meeting, 43rd, Toronto, Ontario, May 8–11, API, Vol. 57, Washington, DC, pp. 509–514.

Prager, M., 1991, "Summary of Frangible Roof Failure Experiences," provided information, Pressure Vessel Research Council, ASME, New York, NY, May 6.

Swanson Analysis Systems, Inc., 1994, *ANSYS Manuals,* Houston, PA.

Swenson, D., Fenton, D., Lu. Z., Ghori, A., and Baalman, J., 1994, "Evaluation of Design Criteria for Storage Tanks with Frangible Roof Joints," Final Report, Kansas State University, Manhattan, KS.

Yoshida, S., and Miyoshi, T., 1992, "Bifucation Buckling of the Top End Closure of Oil Storage Tanks Under Internal Pressure," *Stress Classification, Robust Methods, and Elevated Temperature Design,* ASME PVP-Vol. 230.